FH AACHEN
UNIVERSITY OF APPLIED SCIENCES

Project: Design of 1-D electromagnetic Optical scanner with MEMS micromirror operating in resonate mode for application of LiDAR system

Author: Mr. Saurabh Borse, Mr. Arvind Patel, Mr. Dixie Geraldo

Guided by: Prof. Dr. rer. nat. Klaus-Peter Kämper

FH Aachen University of applied science, Aachen 2022-23

A Research in the field of Micro Electromechanical system for the degree of Master of Science in Mechatronics studies

Contents

Abstract

In recent years, LiDAR has gained significant attention in both academic and industrial sectors due to the increasing demand for autonomous vehicles that require simultaneous mapping and localization. LiDAR is considered a crucial sensor for autonomous driving and flying, as it can provide high-density 3D point clouds with accurate information. In this paper, the figure of merit (FoM) is defined for MEMS mirrors in LiDAR scanners based on aperture size, field of view (FoV), and resonant frequency. The paper provides an overview of Microelectromechanical Systems (MEMS) 1-D scanning mirrors, including different actuation principles and fabrication processes. MEMS mirror-based laser scanners are advantageous in terms of size, speed, and cost compared to other types of laser scanners, making them suitable for LiDAR applications in various fields.

1 Introduction

LiDAR, or Light Detection and Ranging, is a technology for measuring distances using modulated lasers. It was first demonstrated in the 1960s and was initially used in meteorology but has since found applications in a wide range of fields, including autonomous vehicles, agricultural and archaeological surveys [5].

In autonomous vehicles, LiDAR is used for tasks such as obstacle detection, object recognition and tracking, and simultaneous localization and mapping (SLAM) [7]. With the growing demand for autonomous vehicles, the market for LiDAR is rapidly expanding.

LiDAR can be classified into two main categories: non-scanning LiDAR and scanning LiDAR. Non-scanning LiDAR, also known as Flash LiDAR, is the most used type [8]. On the other hand, scanning LiDAR systems steer the laser beam and are more mature, providing higher signal-to-noise ratio compared to Flash LiDAR. Scanning LiDAR can be further classified into two categories: non-mechanical scanning LiDAR and mechanical scanning LiDAR. Non-mechanical scanning LiDAR uses optical phased arrays (OPAs) to steer the laser beam, while mechanical scanning LiDAR, including motorized optomechanical and MEMS scanning LiDAR, employs moving parts for laser scanning [9].

OPAs are a type of solid-state beam steering technology that allows for non-mechanical steering of optical beams. They offer several benefits, such as high stabilization, random-access pointing, and good optical power handling [9]. Flash LiDAR and OPAs are collectively referred to as solid-state LiDAR due to the lack of moving parts in their scanners.

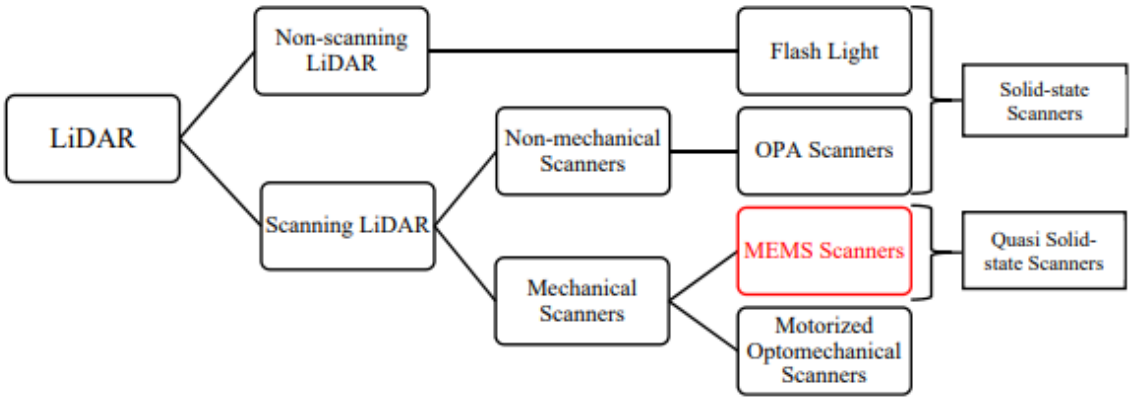

Figure 1.1. Different types of LiDAR scanner [1]

1.1 Non-Scanning LiDAR:

Non-scanning LiDAR is also called Flash LiDAR. “Flash” refers to the idea that the 2D FoV of interest is entirely illuminated by the laser source, like a camera with a flashlight, while an array of photodetectors at the image plane simultaneously picks up the time-of-flight (ToF) information of individual pixels in the 2D FoV as illustrated in Fig. (2a). Flash LiDAR uses all solid-state components, which has the advantages of no moving parts, being resistant to vibrations, a compact size, and low price. Flood illumination implies that each pixel of the photodetector array receives only a small fraction of the returning laser power, leading to a low signal-to-noise ratio (SNR), which greatly limits the distance measurement range or demands very high laser power [8,12]. Furthermore, the resolution of the detector array-based non-scanning LiDAR is constrained by the size and density of the detector array.

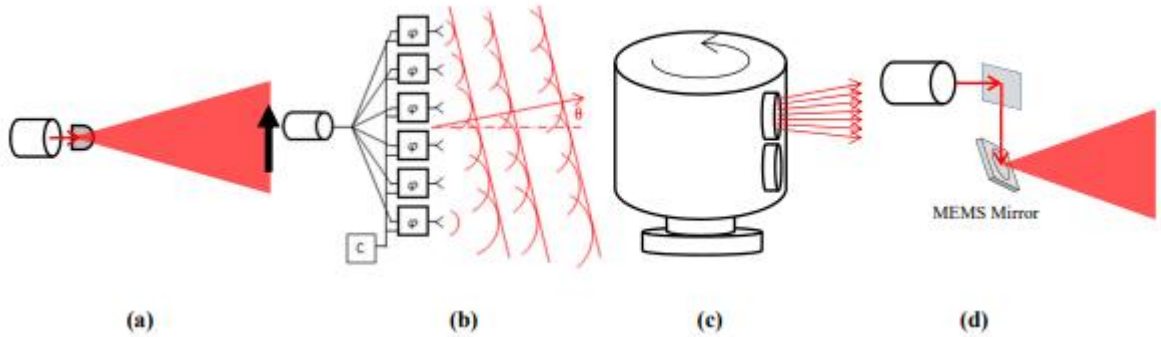

Figure 1.2. (a) A flash LiDAR with diffused light; (b)The principal of an optical phase array (OPA); (c) A LiDAR motorized spinning scanner; (d) A microelectromechanical systems (MEMS) laser scanner [1]

1.2 Scanning LiDAR:

1.2.1 Non- Mechanical Scanning LiDAR:

Laser beam scanning is an important aspect of LiDAR technology, and it can be divided into two categories: non-mechanical scanning and mechanical scanning. Non-mechanical scanning is achieved through optical phased arrays (OPAs) which are a type of solid-state beam steering technology that can steer optical beams without moving parts (as shown in Fig. (2b)) [3]. OPAs have benefits such as high stability, random-access pointing, and good optical power handling. The laser power is divided into an array of transmitters and the phases of each transmitter can be individually controlled. By dynamically adjusting the relative phase shifts among the transmitters, the laser beam can be formed and steered [1]. There are different types of OPAs based on different phase modulators such as liquid crystals, MEMS, or silicon photonics.

Liquid crystal OPA devices have low driving voltage and simple implementation. However, they have a limited maximum scanning angle of around ±10◦ and the steering time is typically several milliseconds, which may not be fast enough for certain LiDAR applications. MEMS-based OPAs, on the other hand, have higher efficiency, faster steering speed and no changes in polarization [1].

Silicon photonic phased arrays have several benefits such as large-scale arrays, compatibility with CMOS processes, high integration, and low cost [1]. S. Chung et al. developed a 1D silicon photonics-based OPA with 1024 elements using a standard 180 nm silicon-on-insulator (SOI) wafer process [13]. The OPA achieved a maximum scanning angle of 45◦ with an angular resolution of 0.03◦ using thermal-optical phase modulation and had a response time of about 66 µs [24]. However, increasing the output optical power of silicon photonics phased arrays to a practical level remains a big challenge [9].

1.2.2 Motorized Optomechanical scanning LiDAR:

Motorized optomechanical scanners, which were popularized by Velodyne's release of the first 64-line LiDAR in 2007, are the most common type of LiDAR scanners [7]. These scanners use multiple channels of transmitters and receivers stacked vertically and rotated by a motor to create a full 360-degree Field of View (FoV) with multiple horizontal lines. While these scanners have a long ranging distance, fast-scanning speed and wide FoV [8], they are not power-efficient and are vulnerable to mechanical shock and wear. In addition, the vertical resolution of these scanners is fixed and dependent on the number of channels, leading to high cost for high resolution.

The high cost of these LiDAR solutions is a hindrance to the progress of autonomous vehicles, as the market and demand for compact LiDAR are rapidly growing. However, current LiDAR solutions based on motorized scanners are either costly, bulky, and demand more power, or perform poorly.

1.2.3 MEMS Mirror-Based Quasi Solid-State LiDAR

As discussed above, both solid-state LiDAR and mechanical scanning LiDAR have major obstacles to overcome before they can be practically used in self-driving cars. Micro-Electro-Mechanical Systems (MEMS) technology provides a viable alternative. MEMS mirrors can steer, modulate, and switch light, as well as control phase. MEMS mirrors have already found enormous commercial success in projectors, displays, and fibre optic communications [8]. The most critical characteristics of MEMS mirrors lie in the fact that they are small and steer light in free space. Thus, compared to motorized scanners, MEMS scanners are superior in terms of size, scanning speed, and cost [9].

In the scheme of a MEMS mirror-based LiDAR, only the tiny mirror plate (whose diameter is in the range of 1–7 mm) of the MEMS device moves while the rest of the components in the system are stationary. Thus, MEMS LiDAR are often referred to as quasi-static-state LiDAR, an ultimate compromise of solid-state LiDAR and mechanical scanning LiDAR. LiDAR laser scanners have different requirements for different application scenarios, which brings both challenges and new opportunities for MEMS mirrors.

Following table summarize the comparison between LiDAR types based on its advantages and disadvantages.

Classification	Advantages	Disadvantages
Flash Lidar	• Solid state non-moving component • Resistant to vibrations • Compact size and low price	• Small fraction of returning laser power • Low SNR – limits the distance measurement range • High laser power • Resolution depends on size and density of detector array
OPA scanners	• High SNR w.r.t flash scanner • High stabilization • Good optical handling power • Array of transmitters whose phase can be controlled	• Liquid crystal OPA: scanning angle limited to +/- 10 deg. Because of low efficiency • High steering time: few milliseconds
Motorized Optomechanical scanners	• Long range • Wide FOV • Fast scanning speed along motorized axis	• Vulnerable to mechanical shocks • High power consumption • High vertical resolution based on no. of transmitter and receiver cannels • costly
MEMS scanners	• Can steer, modulate and control phase of laser • High scanning speed • Cost effective • Compact packaging • Low power consumption	• Vulnerable to mechanical shocks- for motorized based actuation • Based on different actuation principal

Table 1.1. Comparison between different types of LiDAR scanners

2 Figure Of Merit (FOM)

There are several factors that affect the performance of a MEMS mirror. Thus, a Figure of Merit (FoM) that combines multiple critical factors is typically used to determine the suitability of various MEMS mirrors for a specific application.

Example 1: For instance, M. Saleem et al. used a FoM combining the deflection angle, power consumption, and actuator temperature to optimize their electrothermal MEMS mirror design for endoscopic optical coherence tomography (OCT) applications [5].

Example 2: U. Baran et al. defined a FoM as the multiplication of the optical scanning angle, mirror width along the scanning direction, and resonant frequency of scanning mirrors to compare piezoelectric MEMS mirrors for high-resolution displays [6].

In this paper, a FoM is defined as the product of the scan angle, mirror area, and resonant frequency, and will be used to compare various MEMS mirrors for LiDAR applications.The main scanning characteristics of the MEMS mirror include the scanning Field of View (FoV, or θ), scanning optical aperture (i.e., MEMS mirror size 2w), scanning frequency (f), and scanning robustness (corresponding to the resonant frequency of the MEMS mirror, f). These parameters are discussed below, which are then combined to define an FoM.

2.1 Scanning FoV:

The FoV of the LiDAR is the scanning angular range, θ, of the laser scanner if the optical receiver has a sufficiently large acceptance FoV. Different applications have different requirements on FoV. In the case of autonomous driving, the FoV of interest for LiDAR is mainly in the forward direction that the vehicle heads to, which is like the cameras or radars systems used for driving assistance on cars today. In the case of LiDARs for geological survey, the FoV of interested is in the downward direction [11]. Thus, the required FoV for a LiDAR may range anywhere from a few degrees to over 100 degrees.

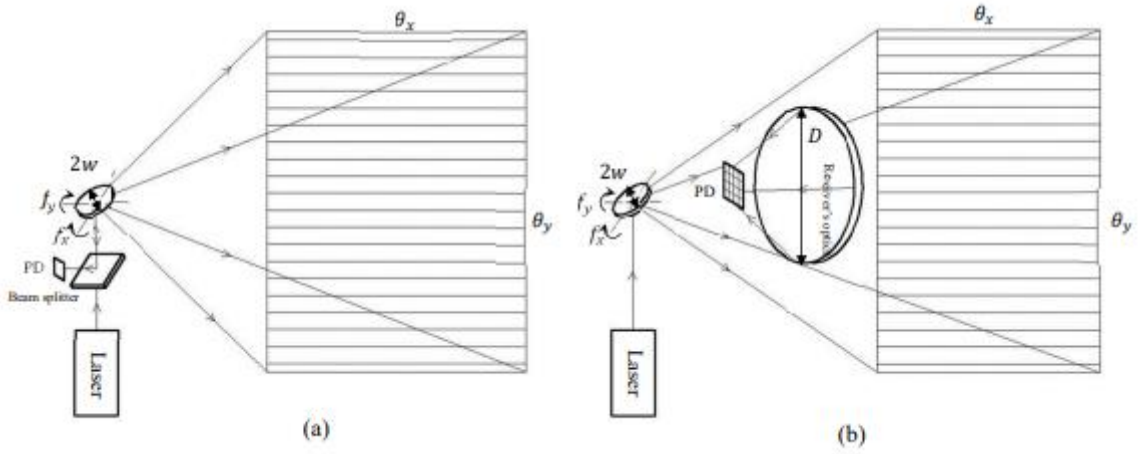

Figure 2.1. The schematics of MEMS scanned LiDAR with (a) coaxial architecture, and (b) non-coaxial architecture. 2w: the dimension of the MEMS mirror plate. fx, fy: the horizontal and vertical scanning frequency of the MEMS mirror. θx and θy: the horizontal and vertical optical scanning FoV. D: the dimension of the receiver's optical aperture [1]

2.2 Scanner's Optical Aperture:

The spatial resolution of LiDAR is determined by the divergent angle of the laser beam, which is given by,

$$\theta_{min} \cong \frac{M^2 \lambda_0}{\pi w_0}$$

Where,

Θ_{min} = is the half divergence angle of the laser beam,

λ_0 = wavelength of the laser,

w_0 = is the half beam waist of the laser (which is usually limited by the MEMS mirror dimension w)

M^2 = is the laser beam quality.

An angular resolution of less than 1 mrad is typically required for LiDAR applications. This will require the scanning mirror plate to have a size of 1 mm for lasers with good beam quality and 3 mm for edge-emitting pulsed laser diodes with poor beam quality [1].

The maximum detectable distance of a LiDAR is determined by the minimum detectable power of the photodetector. The optical power detected by the photodetector is proportional to the receiver's optical aperture, which is given by [1],

$$P_r = P_s \eta_t \times \frac{\rho}{r^2} \times \frac{\pi D^2 \eta_r}{2}$$

Where,

Pr = received signal power (W);

Ps = source laser power (W)

ηt = transmitter optical efficiency

ρ = the reflectivity of the target object

r = range from the transmitter to the target (m)

D = receiver aperture diameter (m)

ηr = receiver optical efficiency

2.3 Scanning Speed and Resonant Frequency:

The frame rate of a LiDAR scanner is determined by the number of scanned frames in the slow axis (vertical) per unit time. The resolution in the fast-axis (horizontal) P_h is determined by the Time-of-Flight (ToF) measurement rate(n) and the fast-axis scanning frequency f_h, while the resolution in the slow-axis is determined by the ratio of the fast-axis scanning frequency and the slow-axis scanning frequency. For a motorized LiDAR with a rotational stage, the fast-axis scanning is usually achieved by quickly switching the laser array on and off in the vertical direction, and the slow-axis scan frequency is the rotation rate of the motor. For MEMS scanned LiDAR for self-driving cars, the fast-axis scanning frequency is typically in the range of 0.5-2 kHz and the slow-axis scanning frequency is typically 10-30 Hz. A balance between fast-axis and slow-axis scanning frequencies must be achieved for a trade-off between resolution and frame rate.

$$p_h = \frac{n}{2f_h}$$

$$p_v = \frac{f_h}{f_v}$$

Where,

Ph = resolution along fast axis

Pv = resolution along slow axis

A MEMS mirror with a high resonant frequency is preferred not only because it can scan fast or obtain high resolutions or high frame rates, but also because higher resonant frequency leads to greater robustness. The resonant frequency of a MEMS mirror is given by[1]:

$$f_0 = \frac{1}{2\pi}\sqrt{\frac{k}{m}}$$

Where m is the equivalent mass and k is the equivalent spring constant of the MEMS mirror. The quality factor (Q factor) of a resonator can be defined as the ratio of the resonator's centre frequency f_0 to its bandwidth Δf [1]:

$$Q = \frac{f_0}{\Delta f_0}$$

The quality factor (Q-factor) of a MEMS mirror determines its susceptibility to changes in its resonant frequency, which affects the scanning angle and phase delay. High Q-factor MEMS mirrors can have large scanning angles at resonance, but their bandwidth is small, making them sensitive to even minor shifts in the resonant frequency. On the other hand, low Q-factor MEMS mirrors are less susceptible to shifts in resonant frequency but require larger quasi-static scan angles. LiDAR systems must operate in dynamic and harsh environments, so real-time monitoring of the environment and feedback control of the MEMS mirror position is necessary to maintain a stable scanning angle.

2.4 Scanner's Size and Weight:

A crucial aspect of laser scanner design for LiDAR is balancing the size and resolution of the optical aperture. Larger apertures result in higher-resolution scans, but smaller apertures are necessary for compact LiDAR systems. Despite their small size and weight, commercially available motor scanned LiDARs are becoming more compact, such as the Velodyne Alpha Prime, which has 128 channels and measures 141 × 165 × 165 mm^3 while weighing only 3.5kg [1].

For robotics applications, compactness is crucial as weight and size restrictions can be stringent, like the Hokuyo UST-10LX LiDAR, which weighs only 130g. In the micro-robotics field, LiDAR scanners must be ultra-small, with some systems weighing under 10g. Using Micro-Electro-Mechanical Systems (MEMS) mirrors can significantly reduce the size and weight of LiDAR scanners. [9]

2.5 Typical Requirements for MEMS Mirror for LiDAR Applications:

As analysed above, the baselines for MEMS mirrors for different applications are summarized in below table based on different research journals and LiDAR which are being used in automotive and other competitive fields. The requirements under other applications are also given based on their working conditions. They are usually less critical than self-driving cars.

Applications	FOV (°)	Mirror Size (mm)	Resonant Frequency (kHz)
Self-Driving Cars	25	2	0.8
Blind-Spot Detection	120	1	0.5
Gesture Recognition	50	0.5	0.2
Ground Robotics	25	1	0.2
Micro Air Vehicles (MAVs)	30	1	0.4

Table 2.1 Application based requirements of LiDAR system [1]

2.6 Figure Of Merit (FoM):

According to the above discussion, the scanning FoV, optical aperture and resonant frequency of a MEMS scanning mirror are the most critical parameters for LiDAR applications. So, a figure of merit (FoM) combining these parameters is defined to evaluate the performance of a MEMS mirror for LiDAR, i.e.,

$$\text{FoM} = \theta e \cdot de \cdot fe$$

$$d_e = \sqrt{\frac{4A}{\pi}}$$

where A is the area of the mirror plate in mm2. For 1D scanning mirrors with a maximum resonant/non-resonant scanning angle of θ0 and resonant scanning frequency of f0, θe and fe are defined as follows,

$$\theta_e = \theta_0 / \beta_{1D}$$

$$f_e = f_0$$

where β1D is a weight factor accounting for the Q-factor for 1D resonant scanning and is defined as, [1]

$$\beta_{1D} = \begin{cases} \log Q & for\ resonant\ scanning \\ 1 & for\ non-resonant\ scanning \end{cases}$$

3 1D MEMS Mirrors:

In this section, we will first discuss the architecture of LiDAR with 1D MEMS mirrors.

3.1 The Architecture of LiDAR with 1D MEMS Mirrors:

The first architecture fig.(4a) consists of a 1D MEMS mirror, a diffuser lens, and a photodetector (PD) 1D array. The horizontally scanned beam from the MEMS mirror is diffused into a laser line, allowing for scanning in both the vertical and horizontal directions. The horizontal resolution is determined by the measurement sampling rate and MEMS mirror scanning frequency, while the vertical resolution is determined by the number of PD elements. This architecture has high horizontal resolution but low vertical resolution, and the maximum detection distance is limited due to the low optical power density and low signal-to-noise ratio (SNR) of the detected signal.

The second architecture fig. (4b) uses an array of laser sources, a 1D MEMS mirror, and a 2D PD array. This architecture can solve the problems of low laser power density and low SNR of the first architecture, making it closer to realizing a commercial LiDAR for autonomous vehicles. However, extra alignment and assembly effort is required to align the multiple lasers with the MEMS mirror plate, and the small size of the MEMS mirror may result in poor angular resolution.

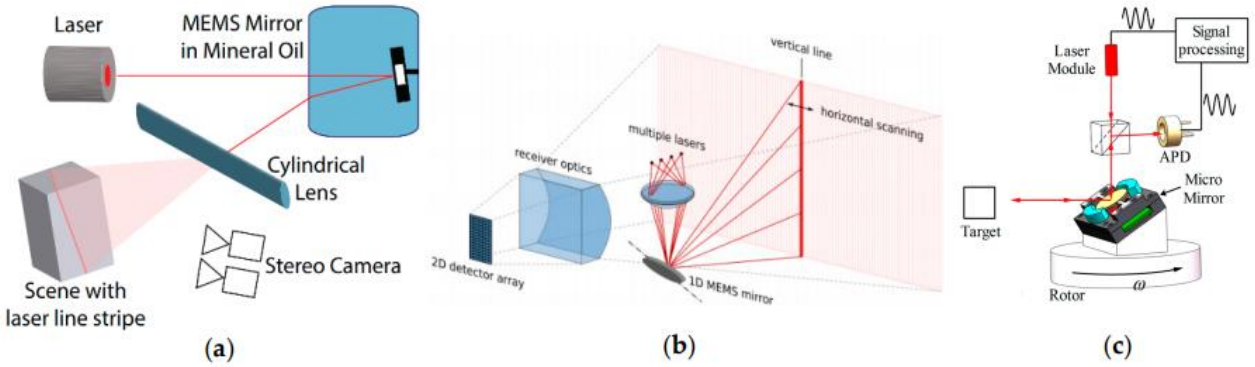

Figure 3.1. (a) The structured light camera design uses an 1D MEMS mirror and diffused laser; (b) The LiDAR designed by Infineon uses a 1D MEMS mirror and a lasers array; (c) The LiDAR with an 1D MEMS mirror and a motor for 2D scanning [1]

A 2D laser scanner can also be created by mounting a 1D MEMS mirror on a motorized 1D scanner, as seen in Fig. (4c). The MEMS mirror and the motorized scanner move in a perpendicular manner, creating a 2D scanning field of view (FoV). The motorized scanner can be a rotary motor and provides the advantage of a wide scanning angle of up to 360 degrees for slow axis scanning. The MEMS mirror, on the other hand, has the benefit of high resonant scanning frequency in the kilohertz range for fast axis scanning. The optical receiver can be designed in a coaxial manner with the transmitted laser, allowing the backscattered light to follow the same path as the transmitted laser. This design requires only one photodetector and simplifies the structure and signal processing units of the LiDAR. However, the maximum detection distance is limited by the size of the MEMS mirror aperture.

LiDAR with 1D Micromirror and diffused laser	LiDAR with 1D Micromirror and laser array	LiDAR with 1D Micromirror and motorized actuation
•Horizontal scanning - Micromirror •Vertical scanning - diffuser lens •Vertical resolution depends on number of photodetector in the array •Cost increases with PD array size i.e. with resolution	•Vertical scanning - Array of laser source •Horizontal scanning b- micromirror actuation •Improved laser power density and SNR •Precise alignment and assembly required to align multiple lasers with micromirror	•Fast axis scanning - micro-mirrors •Slow axis scanning- rotary actuator •Coaxial architecture, one photodetector required •Max. range is limited by aperture size

Table. 3.1 Comparison between different architecture of LiDAR with 1D MEMS Mirror

3.2 Resonant Scanning 1D MEMS Mirrors:

Resonant scanning 1D MEMS mirrors have been widely used for making MEMS LiDAR due to their large angle and relatively high actuation speed. In resonant mode the complex movement of mirror not possible, general behaviour is sine wave irrespective of applied excitation current i.e square wave or sine wave. It is preferred in applications where high speed and constant reciprocating motion is desired. Resonant mode also known as non-linear mode because non-linear output characteristics between drive current and angle of deflection. A feedback control is must to maintain the operating frequency equal to resonance frequency because of change in resonance frequency of mirror because external parameters i.e., temperature, vibration etc.

This 1D resonant scanning electromagnetic MEMS mirror uses a 1D position sensitive detector (PSD) to monitor the scanning angle and provides feedback to the mirror controller, which increases the size and cost of the scanner and LiDAR system. Integrated angular sensing elements can be fabricated directly with MEMS mirrors, such as inductive sensing, piezoresistive sensing, or Hall sensing.

3.3 Non- Resonant scanning 1D MEMS Mirror:

Non-resonant scanning 1D MEMS mirrors have also been widely used for making MEMS LiDAR due to their linearity and robustness. Non-resonant mode also known as linear mode because linear output characteristics between drive current and angle of deflection. It is robust in nature and has large bandwidth. Unlike mirrors operating with resonance mode, the mirror with non-resonating mode does not require feedback control since the change in resonance frequency because of external environmental factors like temperature has no effect on mirror operation. The major disadvantage is the slow speed of operation of micro-mirror in non-resonant mode.

Following table summarises the comparison between the resonant scanning and non-resonant scanning based on different parameters.

Parameter	Resonant scanning	Non-Resonant scanning
Angle of deflection	• Large angle of deflection with less drive current	• Small angle of deflection with same drive current
Robustness	• Less robust, resonance frequency changes with change in environment parameters • External feedback control required to track change in resonance frequency	• More robust, change in resonance frequency of mirror due to change in environmental parameter does not affect the operating point frequency • External feedback control required to track change in resonance frequency
Linearity (Relation between angle of deflection and drive current)	Non- Linear relation between angle of deflection and drive current	Linear relation between angle of deflection and drive current
Drive frequency	Drive current frequency must be equivalent to resonance frequency of micromirror	Drive current frequency in the range of 20 to 50% of resonance frequency of micromirror
Speed of actuation	High speed of actuation	Comparatively low speed of actuation

Table 3.2 Comparison between resonant scanning and non-resonant scanning mode of operation

Conclusion: Non-Resonating mode is more robust, provides better control and high accuracy. Considering the requirements of our application, we chose non-resonant mode of operation.

4 Actuation Principals

Different actuation principals can be used for the actuation of micromirror like electrostatic, electromagnetic, piezoelectric etc. Considering the application requirements i.e. The torque to turn and deflection of the mirror from its mean position, the available options can be narrowed down to two important principals: 1) Electrostatic and 2) Electromagnetic.

4.1 Comparison Between Electrostatic and Electromagnetic Mode of Actuation:

4.1.1 Electrostatic Actuation

Electrostatic actuation is based on the principle of electrostatic attraction between two oppositely charged plates, depicted in Figure 2-3 (Coulomb's law) where the electrostatic force, F_{es} between two plates is given by:

$$F_{es} = \frac{A\varepsilon V^2}{2f_g^{\,2}}$$

where A is plate overlap area, V is the potential difference, ε is the dielectric permittivity of the medium and f_g is the gap between the two plates.

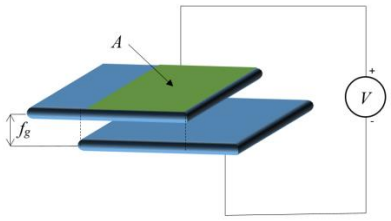

Figure 4.1. Schematic –Electrostatic actuation between two oppositely charged plates actuation [3]

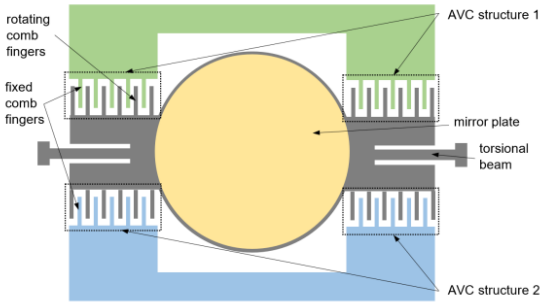

Figure 4.2. Illustration of the scanning micro-mirror designed by ST Microelectronics to operate at fr = 21.5 kHz, θmax = 12° at a drive voltage amplitude of 200 V [3]

Following table summarises the advantages and disadvantages of electrostatic actuation mode for micromirror actuation.

Advantages	Disadvantages
Low power consumption: Electrostatic actuation requires relatively low power compared to other actuation principles	**Sensitive to environmental factors**: Electrostatic actuation can be sensitive to environmental factors such as temperature, humidity, and atmospheric pressure
Non-contact operation: Electrostatic actuation operates without physical contact, which can reduce wear and tear and improve the lifespan of the device	**Limited displacement**: Electrostatic actuation typically has limited displacement, which limit its application
High precision: Electrostatic actuation can achieve high precision motion due to its fine control over the electrostatic force	**Pull-in instability**: Electrostatic actuation can suffer from pull-in instability, where the electrodes come into contact and stick, leading to device failure
	Electrostatic noise: Electrostatic actuation can generate electrostatic noise, which can impact the performance and accuracy of the device

Table 4.1 Advantages and disadvantages of electrostatic mode of actuation

4.1.2 Electromagnetic Actuation

Following figure illustrate the actuation of micro-mirror using electromagnetic actuation principal using with Lorentz force and the table below it compares the advantages and disadvantages of electromagnetic actuation principal.

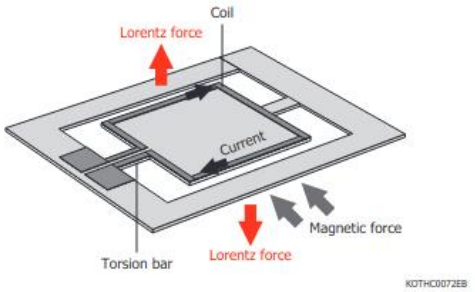

Figure 4.3. Schematic – Electromagnetic actuation of micro-mirror using Lorentz force for actuation designed by Hamamatsu electronics [2]

Mathematically, following equation elaborates the relation between the resultant torque, drive current and the mirror dimensions is given by:

$$M_{EM} = 2\sum_{n=1}^{N} F_{lor} r_n = 2\sum_{n=1}^{N} Bil_n r_n$$

Where,

B = the magnetic field
I = the drive current
ln = the conductor length,
N = the number of coils turns,
r_n = the distance of the nth coil turns from the center

Advantages	Disadvantages
Large displacement: Electromagnetic actuation can produce large displacement, making it suitable for applications requiring large motion	**High power consumption**: Electromagnetic actuation requires a significant amount of power, which can limit its use in low-power applications
High speed operation: Electromagnetic actuation can achieve high-speed operation, making it suitable for applications requiring fast motion	**Complex fabrication**: Electromagnetic actuation requires complex fabrication processes, which can increase the cost and complexity of the device
High force generation: Electromagnetic actuation can generate high forces, making it useful in applications requiring high-force actuation	**Magnetic interference**: Electromagnetic actuation can produce magnetic interference, which can impact the performance of other nearby devices
Durability: Electromagnetic actuation can provide long-term durability, as the magnetic field can be maintained over extended periods of time without degradation	**Reliance on magnetic materials**: Electromagnetic actuation relies on magnetic materials, which may have limited availability and may not be suitable for all applications
Easy integration: Electromagnetic actuation can be easily integrated with other micro-electromechanical systems (MEMS) components, making it a useful addition to many MEMS devices	
High reliability: Electromagnetic actuation can be highly reliable, as the magnetic field can be precisely controlled and maintained	

Table 4.2. Advantages and disadvantages of electromagnetic mode of actuation

Conclusion: Electromagnetic actuation is suitable for high-speed operation along with large possible displacement. Considering the force and displacement requirements, we chose electromagnetic actuation for this application.

5 Calculation

5.1 Micro-mirror Design Calculation

In order to soothe the fabrication of the system by bulk micro-machining on silicon wafer, and also to fulfil certain parameters as stated in **Table 5.1**:

Parameters	Target
Scanning Angle	≥ ±30°
Resonance Frequency	≥ 500Hz
Mirror Size	≥ 3mm x 3mm
Surface Flatness	≤ 200 nm

Table 5.1. Specification parameters for 1D electromagnetic micro-mirror operating in resonant mode

Therefore, we decided to go with a rectangular cross-section micro-mirror with total area of 9mm² and thickness of 0.1mm. We can obtain the mass of the mirror system simply by:

$$m_{mirror} = V_{mirror} \times \rho$$
$$V_{mirror} = A_{mirror} \times t_{mirror}$$
$$V_{mirror} = 9mm^2 \times 0.1mm = 0.9mm^3$$
$$m_{mirror} = 0.9mm^3 \times 2330 \times 10^{-9} \frac{kg}{mm^3} = 2.097 \times 10^{-6} kg$$

Where,

t_{mirror} = thickness of the mirror (mm)
A_{mirror} = area of the rectangular cross-section (mm^2)
V_{mirror} = volume of the mirror (mm^3)
m_{mirror} = mass of the mirror (kg)
ρ = Monocrystalline Silicon [100] density ($2330 \times 10^{-9} kg/mm^3$)

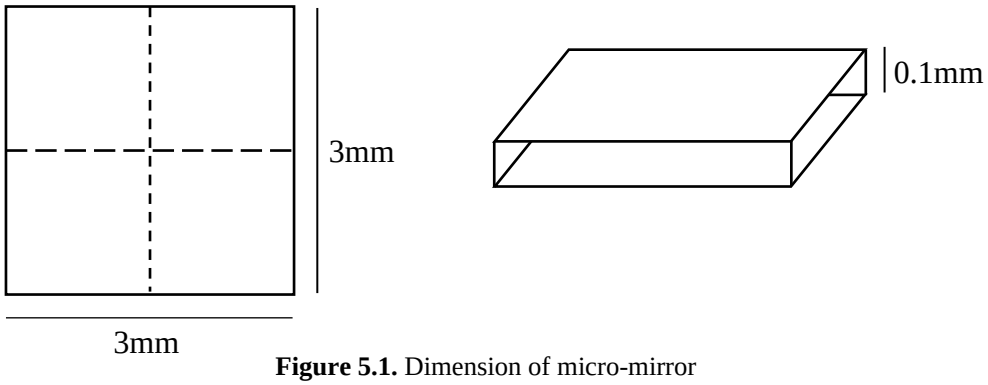

Figure 5.1. Dimension of micro-mirror

Besides the mirror, we also consider the mass of 2 rectangular cross-section beam which located at the left and right of the mirror and the dimension of each beam is 0.5mm x 0.1mm x 2.2mm. Thus, the volume and mass of the beam can be obtained in a similar way of the mirror.

$$m_{beam} = V_{beam} \times \rho$$
$$V_{beam} = w_{beam} \times l_{beam} \times t_{beam}$$
$$V_{beam} = 0.5mm \times 2.2mm \times 0.1mm = 0.11mm^3$$
$$m_{beam} = 0.11mm^3 \times 2330 \times 10^{-9} \frac{kg}{mm^3} = 2.563 \times 10^{-7} kg$$

Where,

w_{beam} = width of the beam (mm)
l_{beam} = length of the beam (mm)
t_{beam} = thickness of the beam (mm)
V_{beam} = volume of the beam (mm^3)
m_{beam} = mass of the beam (kg)
ρ = Monocrystalline Silicon [100] density ($2330 \times 10^{-9} kg/mm^3$)

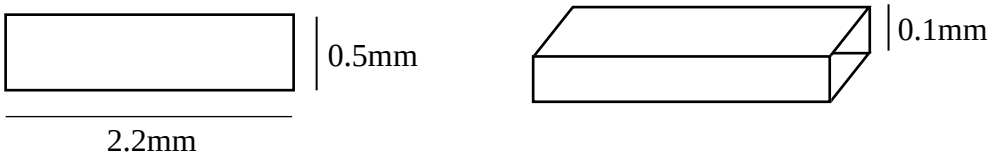

Figure 5.2. Dimension of beam

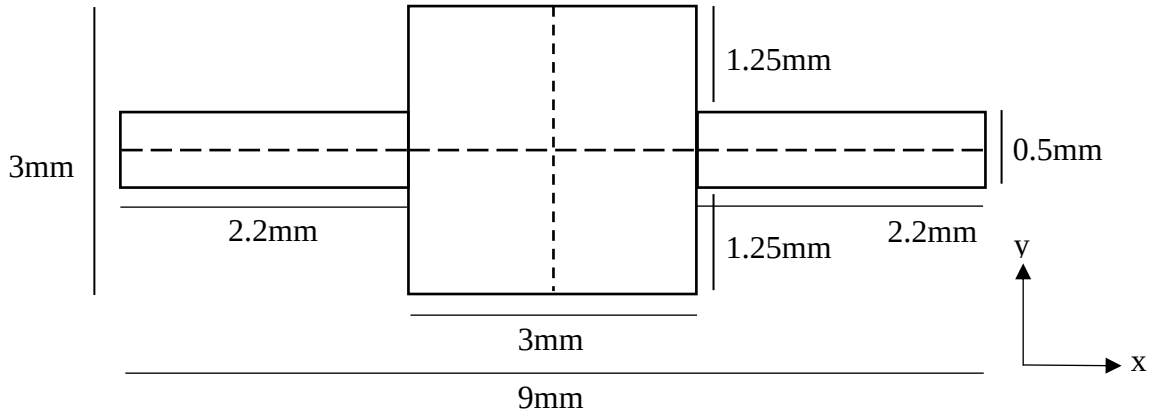

Figure 5.3. Dimension of the system

When the system operates in non-resonating frequency region of 250Hz, to achieve scanning angle of 30°, it will generate torque to the system beams. To analyse the torque acting on the system, we first need to determine the total mass moment of inertia acting on the system and the rotation angle it will generate. These 2 quantities can be calculated by:

1. Total mass moment of inertia of half the system

$$I_{total} = \frac{1}{2} I_{mirror} + \frac{1}{3} I_{beam}$$

Half of the system is used to simplify the analogy and calculation of the system. The system consists of 2 different geometries: rectangular for the mirror and square for the beam that rotates in x axis, which denotes by:

$$I_{mirror} = \frac{1}{12} \times m_{mirror} \times {l_{mirror}}^2$$

$$I_{beam} = \frac{1}{12} \times m_{beam} \times {l_{beam}}^2$$

$$I_{mirror} = \frac{1}{12} \times 2.097 \times 10^{-5} kg \times 3mm^2 = 1.573 \times 10^{-6} kgmm^3$$

$$I_{beam} = \frac{1}{12} \times 2.563 \times 10^{-7} kg \times 0.5mm^2 = 5.340 \times 10^{-9} kgmm^3$$

Thus, the total moment of inertia of half system is:

$$I_{total} = \left(\frac{1}{2} \times 1.573 \times 10^{-6}\right) kgmm^3 + \left(\frac{1}{3} \times 5.340 \times 10^{-9} kgmm^3\right)$$
$$= 7.881 \times 10^{-7} kgmm^3$$

2. Rotation angle of the system

$$\varphi = \frac{r}{l_{beam}} \times \theta$$

$$r = \sqrt{\frac{{w_{beam}}^2}{2} + \frac{{t_{beam}}^2}{2}}$$

$$r = \sqrt{\frac{(0.5mm)^2}{2} + \frac{(0.1mm)^2}{2}} = 0.255mm$$

$$\varphi = \frac{0.255}{2.2} \times 30 \times \frac{\pi}{180} = 0.061$$

Where,

φ = rotation angle (radian)

θ = scanning angle (radian)

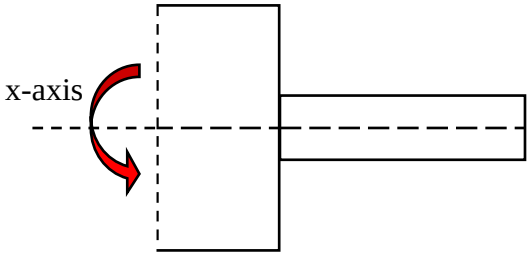

Figure 5.4. Half of the system rotates in x-axis

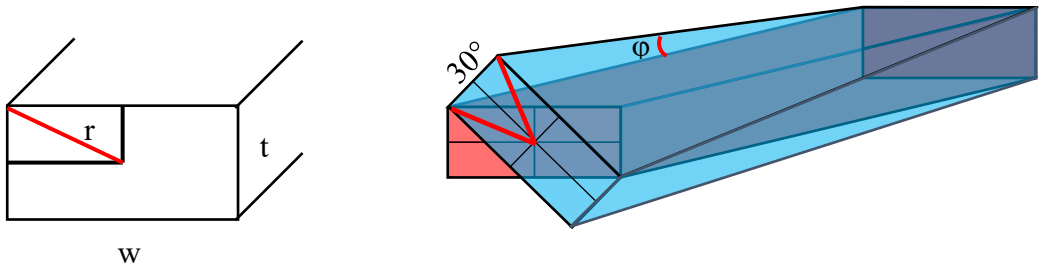

Figure 5.5. Rotation angle (φ) generate by 30° scanning angle (θ)

Then, we use equilibrium methods for determining natural frequency of free torsional vibrations. Given the diagram below, where the shaft end represents our micro-mirror beam end that are fixed, and the weight as the half of our micro-mirror:

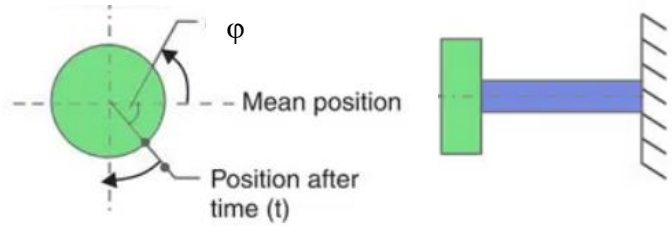

Figure 5.6. Shaft where the end is fixed and the other is attached to a body of weight W

When the body is in equilibrium position it generates:

1. Accelerating force $= I \times \frac{d^2\varphi}{dt^2}$
2. Restoring force $= q \times \varphi$

and by relating the accelerating force to restoring force after time t, yield us a relation of:

$$I \times \frac{d^2\varphi}{dt^2} = -q \times \varphi$$

$$\frac{d^2\varphi}{dt^2} + \left(\frac{q}{I} \times \varphi\right) = 0$$

while noting that the fundamental of simple harmonic motion is:

$$\frac{d^2x}{dt^2} + (\omega^2 \times x) = 0$$

Thus, we can see that by equating these similar equations, we end up with:

$$\omega = \sqrt{\frac{q}{I}} \text{ or } f_n = \frac{1}{2\pi}\sqrt{\frac{q}{I}}$$

Where,

ω = angular frequency (radian/s)
f_n = natural frequency (Hz)
q = torsional stiffness of the beam (kgmm^2/s^2)
I = mass moment of inertia (kgmm^3)

We then apply this relation to our system, with reference to 1D micro-mirror manufactured by Hamamatsu, the mirror can be operated in between the 20 to 50% of natural frequency for non-resonant mode. Since we used non-resonant mode, the operating frequency of our system is 250 Hz and the total mass moment of the system is 7.881x10^{-7}kgmm^3. Thus, we can find the torsional stiffness of beam by:

$$f_n = \frac{1}{2\pi}\sqrt{\frac{q}{I}}$$
$$q = (f_n \times 2\pi)^2 \times I_{total}$$
$$q = (250Hz \times 2\pi)^2 \times 7.881 \times 10^{-7} kgmm^3 = 1.944 kgmm^2/s^2$$

and from torsional stiffness, we can finally determine the Torque acting on the system by:

$$q = \frac{T}{\varphi}$$
$$T = q \times \varphi$$
$$T = \frac{1.944 kgmm^2}{s^2} \times 0.061 = 0.118 kgmm^2/s^2$$

After obtaining the torque acting to the system, we can further analyse the system properties of shear stress to make sure the material properties used which is monocrystalline silicon [100] is able to sustain it, and also the force needed so the system can operate in wanted condition. The shear stress generated by the torque on a rectangular cross-section beam can be calculated by

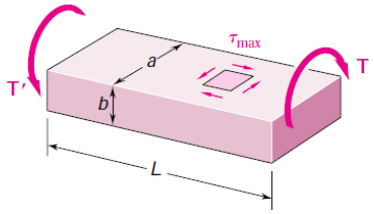

Figure 5.7. Shear stress on a rectangular cross section beam [16]

a/b	c_1	c_2
1	0.208	0.1406
1.2	0.219	0.1661
1.5	0.231	0.1958
2	0.246	0.229
2.5	0.258	0.249
3	0.267	0.263
4	0.282	0.281
5	0.291	0.291
10	0.312	0.312
Infinite	0.333	0.333

Table 5.2. Coefficient for Rectangular Bars in Torsion [16]

$$\tau_{max} = \frac{T}{c_1 ab^2}$$

$$\tau_{max} = \frac{0.118 kgmm^2/s^2}{0.291 \times 0.5mm \times (0.1mm)^2} = 81.100 kg/mms^2$$

Where,

a	= width of the beam (mm)
b	= thickness of the beam (mm)
c_1	= coefficient of rectangular bars in torsion (From **Table 5.2.**)
τ_{max}	= maximum shear stress (kg/mms^2)
T	= torque (kgmm^2/s^2)

The system will have a maximum shear stress of 81.100kg/mms^2 or 0.0811MPa. The maximum shear stress of monocrystalline [100] is 1.7Gpa which concludes that the maximum shear stress generated by the torque is much lower than the maximum shear stress of material being used. Thus, the material will not cause problem for the micromirror to operate.

For simplification, we calculate the force needed of the half system. The force needed by the system to operate, can be evaluated from the torque generated by the system in 250Hz operational frequency, achieving 30° scanning angle by:

$$F = \frac{T}{L/2}$$

$$F = \frac{0.118 kgmm^2/s^2}{\left(\frac{3}{2}\right) mm} = 0.078 kgmm/s^2$$

Whereas the magnetic strength needed to generate 0.078kgmm/s^2 from the permanent magnet on 50mA is given by:

$$B = \frac{F}{I \times (L/2)}$$

$$B = \frac{0.078 kgmm/s^2}{0.05A \times \left(\frac{3}{2}\right) mm} = 0.293T$$

Where,

B	= magnetic field strength

In which we found a N42 neodymium magnet that can sustain our system when operating with width x length x thickness dimension of 3.175mm x 3.175mm x 1.587mm respectively. In which the magnet will have surface magnetic field of 0.44T and 0.320T when it reaches the middle of the wire (0.514mm from the surface of magnet), which was simulated by online simulator of K&J Magnetics, Inc.

Figure 5.8. N24 Rectangular Neodymium magnet specification. Source: https://www.kjmagnetics.com/proddetail.asp?prod=B221 [17]

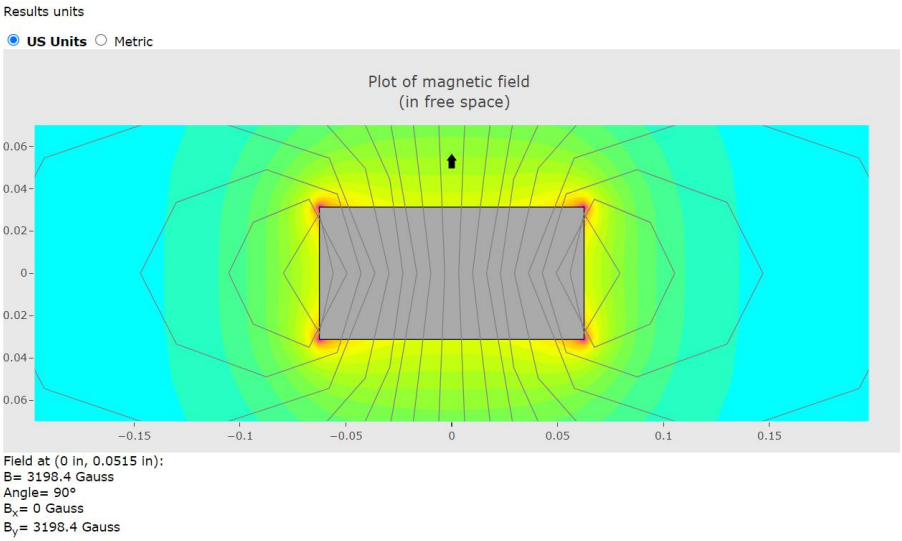

Figure 5.9. Plot of Magnetic Field of Rectangular N24 Neodymium Magnets at The Center of Wire. Source: https://www.kjmagnetics.com/fieldcalculator.asp?calctype=block [17]

For the dimension calculation of the copper wire that will be deposited on to the back of the mirror, we are using online references to help us determine it. Below we obtained the cross-section area of the copper operating in 5V and 50 mA which is 0.00018343mm^2.

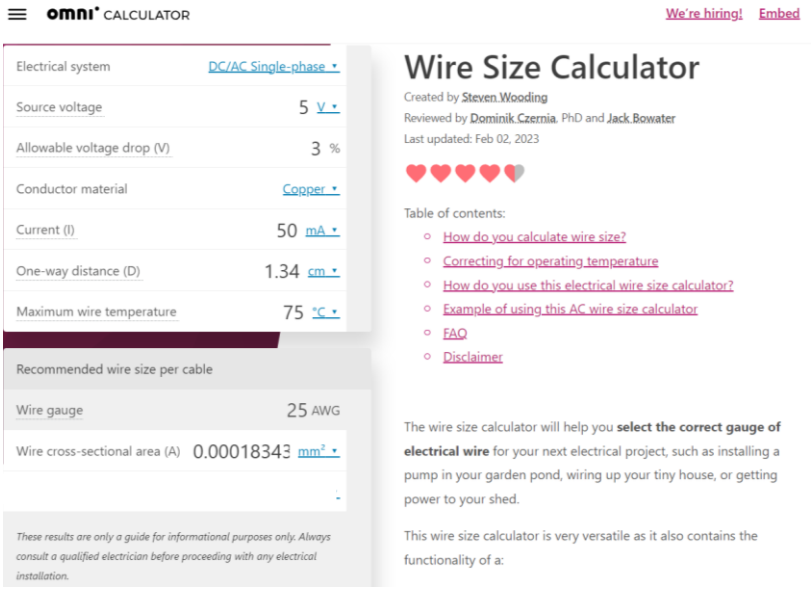

Figure 5.8. Copper wire size calculation. Source: https://www.omnicalculator.com/physics/wire-size [18]

Thus, taking ratio of 20, we got the result of the thickness and width for the rectangular cross-section for the electrical wire as ~0.004mm (4.282µm) and 0.042mm (42.829µm) respectively.

5.2 Figure of Merit (FoM) calculation

As we already mentioned about figure of merit (FoM) as our 1D electromagnetic micro-mirror for LiDAR performance evaluation, we calculated our design scanning FoV, optical aperture, and resonant frequency to compare it with other MEMS mirror for LiDAR, i.e.

$$FoM = \theta e \times de \times fe$$

First, we evaluated our design effectiveness dimension in mirror plate by calculating its optical aperture (d_e) with:

$$d_e = \sqrt{\frac{4A}{\pi}}$$

$$d_e = \sqrt{\frac{4 \times 9mm^2}{\pi}} = 3.385mm$$

Where,

A = area of the mirror (mm^2)

Also, natural frequency of mirror is 500 Hz, thus,

$$f_e = f_0 = 500Hz = 0.5kHz$$

Lastly, effective field of view (θ_e) of our system is 60°. Even though, our system target parameter is 30°, its only applied in 1 direction of mirror, whereas when the mirror operating it will operate in 2 directions back and front. Thus, by:

$$\theta_e = \frac{\theta_0}{\beta_{1D}}$$

$$\beta_{1D} = \begin{cases} logQ & For\ resonant\ scanning \\ 1 & For\ non\text{-}resonant\ scanning \end{cases}$$

$$\theta_e = \frac{60° \times \frac{\pi}{180}}{1} = 1.047\ rad$$

Where,

θ_0 = field of view (radian)

Thus, from scanning FoV (θ_e), optical aperture (d_e), and resonant frequency relationship (f_e), we calculated figure of merit relation for our system as follow:

$$FoM = 1.047 \times 3.385 \times 0.5 = 1.772$$

We will now compare our FoM results with other research published by the other researchers for 1D non-resonant scanning micro-mirror. **Table 5.3** gives you the FoM summary obtained by other researchers.

Marker	Actuation Method	FoM	Mirror Plate Dimension	Non-Resonant Scanning Angle θ		Resonant Frequency f_0 (kHz)	Ref.
				(°)	(rad)		
●	EM	2.44	3.6 × 4.7 mm^2	20	0.35	1.5	[67]
■	EM	2.40	3.6 × 8.5 mm^2	20	0.35	1.1	[67]
▼	EM	0.89	D = 14.2 mm	20	0.35	0.18	[71]
▲	EM	0.11	28.5 mm^2	6	0.10	0.19	[62]
●	ES	1.11	0.8 × 0.8 mm^2	16	0.28	4.4	[66]
■	ES	0.30	D = 1 mm	28.8	0.50	0.6	[68]
▲	ES	0.09	1 × 1 mm^2	18.8	0.33	0.23	[47]
▼	ES	0.04	0.96 × 0.11 mm^2	6.5	0.11	1.1	[72]
●	ET	1.28	0.8 × 0.8 mm^2	180	3.14	0.45	[69]
★	ET	0.83	1 × 1 mm^2	124	2.16	0.34	[73]
▼	ET	0.32	6 × 6 mm^2	15	0.26	0.18	[70]
▲	ET	0.31	0.7 × 0.32 mm^2	30	0.52	1.1	[61]
■	ET	0.29	10 × 10 mm^2	10	0.17	0.15	[70]

Table 5.3. The FoMs of 1D non-resonant scanning micro-mirror system published by other reaserchers [1]

Actuation Method	**FoM**	**Mirror Plate Dimensions**	**Non- Resonant scanning angle**		**Resonance frequency (KHz)**
			(o)	(rad)	
EM	1.772	3 x 3 mm^2	30	0.52	0.5

Table 5.4. The FoM and other parameters of our micro-mirror system

Conclusion: FoM of our system is in range with the designs published by the other researchers for 1D non-resonant micro-mirror with electromagnetic actuation.

6 Fabrication

Considering the fabrication process, we will be manufacturing the micro-mirror along with drive coil of copper and reflective surface of aluminium by multiple lithography and etching process. Followed by gluing the silicon wafer with Pyrex glass cap by anodic bonding, finally the permanent magnets will be placed in the Pyrex glass box completing the assembly.

Below is the stepwise manufacturing process for the complete fabrication of the assembly:

Step 1 (BS) : The system will be fabricated on a 20 μm-thick Silicon wafer.

Step 2 (BS) : The wafers are coated with UV-sensitive photoresist and lithographically patterned by exposing to UV light, then the exposed area is removed (using developer) leaving behind a patterned photoresist.

Step 3 (BS) : A thin layer of copper metal is deposited over the photoresist by the sputtering deposition process. The coil structure and electrical contacts (bond pads) are formed after the lift-off process. Copper electrical contact pads were patterned selectively on the features created in step 2.

Step 4 (BS) : The coil structure is realized after the lift-off process.

Step 5 (FS) : The wafers are coated with UV-sensitive photoresist and lithographically patterned by exposing UV light, then the exposed area is removed (using developer) leaving behind a patterned photoresist.

Step 6 (FS) : A thin layer of Aluminium metal is deposited over the photoresist by the sputtering deposition process. The mirror structure is formed after the lift-off process.

Step 7 (FS) : The wafers are coated with UV-sensitive photoresist and lithographically patterned by exposing UV light, then the exposed area is removed (using developer) leaving behind a patterned photoresist mask for etching.

Step 8 (FS) : A Deep reactive ion etching (DRIE) is used to etch completely through the wafer layer to release the micromirror, after etching, the photoresist is removed.

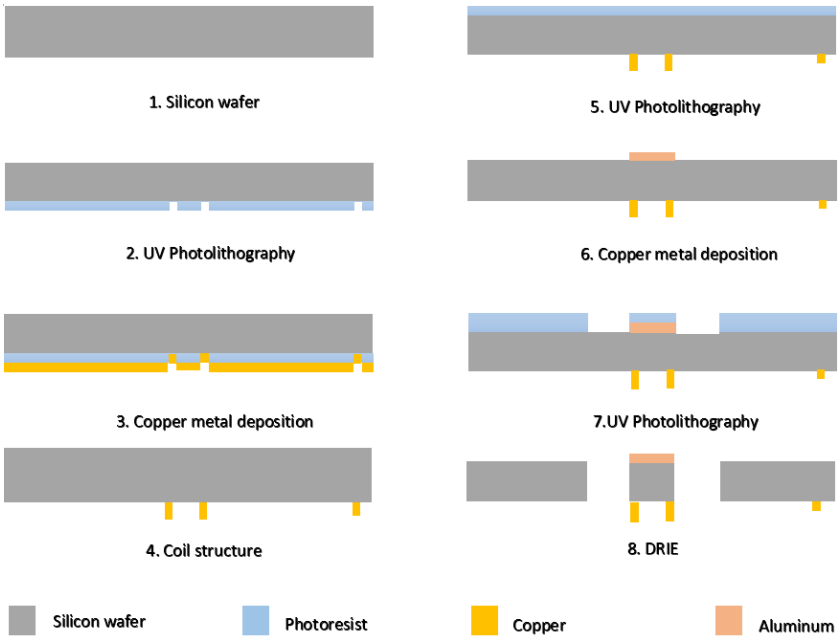

Figure 6.1. Fabrication processes of 1D micromirror.

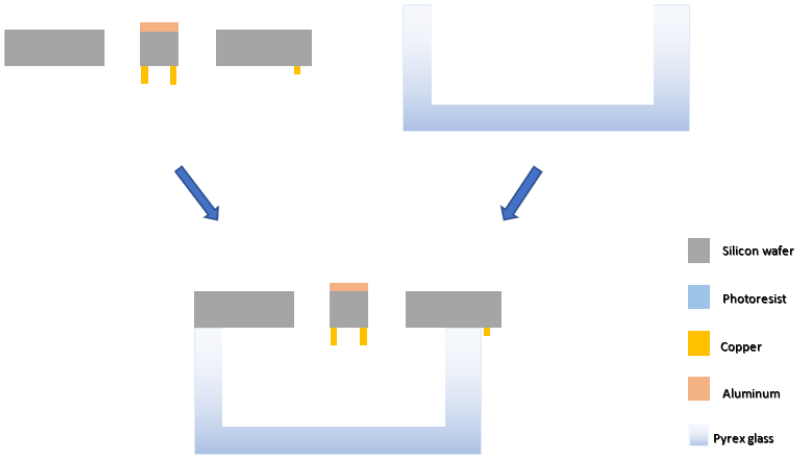

Figure 6.2. Bonding processes of 1D micromirror

The final step of the process is the attachment of the permanent magnet to the Pyrex glass box. The fabricated micromirror and the Pyrex glass are bonded together through an anodic bonding process.

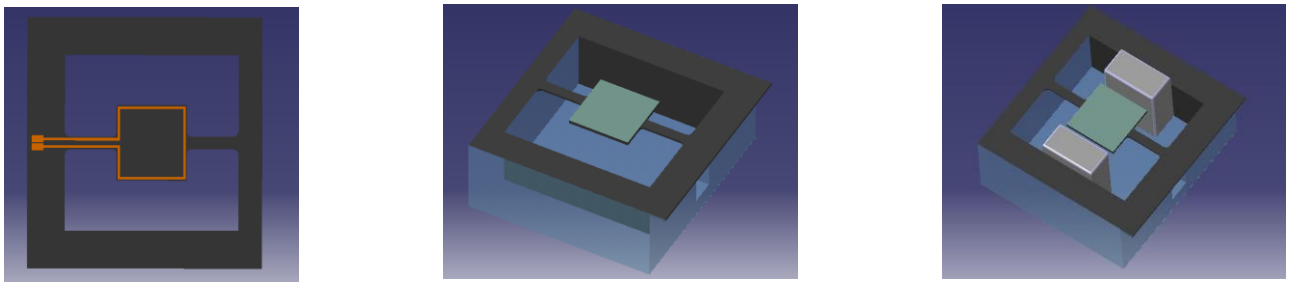

Figure 6.3. 3D view of 1D micromirror

7 References

1. Dingkang wng, Connar Watkins and Huikai Xie, MEMS Mirrors for LiDAR: A Review, Department of Electrical and Computer Engineering, University of Florida, Gainesville, FL 32611, USA, MDPI, 27th April2020
2. MEMS Mirror, Technical information brochure, Hamamatsu, S12237-03P
3. Russell Farrugia; Design, and optimisation of high-performance resonating micro scanners through multiphysic investigation, University of Malta, December 20219
4. G. Amor, E. Roth, D. Sharon, Multiple MEMS mirror synchronization techniques, modelling and applications, ST Microelectronics Ltd.
5. Badarinath, K.; Kharol, S.K.; Sharma, A.R. Long-range transport of aerosols from agriculture crop residue burning in Indo-Gangetic Plains—A study using LIDAR, ground measurements and satellite data. J. Atmos. Solar Terr. Phys. 2009
6. Hening, S.; Ippolito, C.A.; Krishnakumar, K.; Stepanyan, V.; Teodorescu, M. 3D LiDAR SLAM Integration with GPS/INS for UAVs in Urban GPS-Degraded Environments. AIAA Inf. Syst. AIAA Infotech Aerosp. 2017
7. Maturana, D.; Scherer, S. VoxNet: A 3D Convolutional Neural Network for real-time object recognition. In Proceedings of the 2015 IEEE/RSJ International Conference on Intelligent Robots and Systems (IROS), Hamburg, Germany, 28 September–2 October 2015
8. Miyasaka, T.; Ohama, Y.; Ninomiya, Y. Ego-motion estimation and moving object tracking using multi-layer LIDAR. In Proceedings of the 2009 IEEE intelligent vehicles symposium, Xi'an, China, 3–5 June 2009
9. U. Hoffmann, J. Janes, H. Quenzer, High-Q MEMS resonator for laser beam canning displays, Fraunhofer institute for silicon technology, micromachines 2012
10. cala, A. How Multi-Beam Flash Lidar Works. Available online: https://ouster.com/blog/how-multi-beamflash-lidar-works.
11. Liu, J.; Sun, Q.; Fan, Z.; Jia, Y. TOF Lidar Development in Autonomous Vehicle. In 2018 IEEE 3rd Optoelectronics Global Conference (OGC); Institute of Electrical and Electronics Engineers (IEEE): Piscataway, NJ, USA, 2018
12. P. Patterson, D. Hah, M. Fujino, Scanning micromirror: an overview, Japan 2017
13. C. Gorecki, S. Bargiel, MEMS Scanning mirror for optical coherence tomography, HAL open science, id: hal-03814525
14. D. Bayat, Large hybrid high precision MEMS mirrors, Ecole Polytechnique Federale De Lausanne, 2011
15. Philip Kaufmann, A novel indirect actuation concept for MEMS micromirrors, Technischen Uiversitat Chemnitz, Sept. 2019
16. F. Beer; E. Johnston; J. DeWolf; d.Mazurek; Mechanics of Material, McGreaw Hill, 5th Edition
17. K&J Magnetics: B221. (n.d.). K&J Magnetics,Inc. https://www.kjmagnetics.com/
18. Wooding, S. (2023, February 2). Wire Size Calculator. https://www.omnicalculator.com/physics/wire-size